Applied Thermal Engineering 51 (2013) 255–261

Contents lists available at SciVerse ScienceDirect

Applied Thermal Engineering

journal homepage: www.elsevier.com/locate/apthermeng

Temperature-dependent infrared properties of Ca doped (La,Sr)MnO_3 compositions with potential thermal control application

Desong Fan, Qiang Li*, Yimin Xuan, Hong Tan, Junfei Fang

School of Energy and Power Engineering, Nanjing University of Science and Technology, Xiao Ling Wei 200, Nanjing, Jiangsu 210094, PR China

HIGHLIGHTS

- ► Infrared properties of Ca doped (La,Sr)MnO_3 compositions are investigated.
- ► These compositions exhibit a tunable infrared properties basing on their temperature.
- ► The potential application of the compositions in thermal management is discussed.

ARTICLE INFO

Article history:
Received 18 January 2012
Accepted 15 July 2012
Available online 7 September 2012

Keywords:
Manganese oxides
Thermal control
Infrared reflectivity
Infrared emissivity
Metal–insulator transition

ABSTRACT

The synthesized compositions $La_{0.7}Ca_{0.3-x}Sr_xMnO_3$ show their potential in thermal control application. The crystal structure, surface morphology, and the temperature dependence of resistivity, infrared spectra and emissivities for the compositions are reported. All of the synthesized compositions exhibit the characteristics of perovskite structure and of metal–insulator transition. Crystal structure of the compositions changes from the orthorhombic to the rhombohedral structure with increasing doping level (x). The infrared properties of compositions can be automatically adjusted basing on variation in temperature. In the temperature range 97–373 K, the variation amplitude of infrared emissivity exceeds 0.5. The potential application of the compositions in thermal management is discussed.

1. Introduction

Spacecraft in orbit are subjected to space environment temperature fluctuation. In order to maintain all the component of spacecraft within their respective temperature range, an efficient thermal control system is necessary [1]. Thermal control coating is one of the popular materials to be used in the thermal control system. It can achieve a temperature balance in spacecraft by adjusting its thermal infrared properties, such as spectral reflectivity and emissivity, which determine the heat rejection of spacecraft. Since traditional thermal control coating has fixed thermal infrared reflectivity and emissivity, such as OSR and Aluminum, it requires a large and complex temperature control system to adjust the heat rejection in response to temperature fluctuation. This inevitably increases the costing and bulkiness of thermal control system. One expected solution is to develop an advanced thermal control material that can adjust its thermal infrared properties automatically in response to variation in temperature without additional power consumption and moving parts.

Perovskite-type manganese oxides doped with alkaline-earth elements display such properties [2–4]. Recent studies showed their potentiality for thermochromic devices due to their metal–insulator (MI) transitions. For example, in the vicinity of $x = 0.2$, manganese oxides $La_{1-x}Sr_xMnO_3$ showed remarkable emissivity increase upon heating [4–7]. In addition, J. Huang et al. [8] theoretically investigated the thermal radiative properties of structured material $La_{0.825}Sr_{0.175}MnO_3$ combined with Al and SiO_2 gratings and their research indicated that emissivity increment is enhanced in the entire calculated temperature range for the structured surface. These investigations mainly focused on manganese oxides (La,Sr)MnO_3, especially Sr doping level $x = 0.175$. For the manganese oxides $La_{0.825}Sr_{0.175}MnO_3$, it exhibit abrupt metal–insulator transition at $T_{MI} = 283$ K [4]. Though such composition could be a potential candidate for thermal control material, the T_{MI} remain low for applications. The $La_{0.7}Ca_{0.3-x}Sr_xMnO_3$ (LCSMO) is also interesting especially for the Ca rich composition. The magnetoresistance effect behavior of this composition has been already studied in Ref. [9]. The LCSMO compositions also exhibit a low emissivity below the transition temperature T_{MI} and a high emissivity above T_{MI}. The T_{MI} can be adjusted close to room temperature by appropriate Ca:Sr ratio. If the material is coated to the surface of

* Corresponding author. Tel.: +86 025 84315488.
E-mail address: liqiang@mail.njust.edu.cn (Q. Li).

1359-4311/$ – see front matter © 2012 Elsevier Ltd. All rights reserved.
http://dx.doi.org/10.1016/j.applthermaleng.2012.07.046

spacecraft, it can adjust the surface temperature by changing its emissivity. With this mechanism, our study is motivated to provide additional knowledge on the properties of manganese oxides.

In this work, the characteristics of resistivity, infrared emissivity, and spectral reflectivity for the $La_{0.7}Ca_{0.3-x}Sr_xMnO_3$ ($x = 0.1$, 0.12, 0.135, and 0.15) compositions at various temperature are investigated. For further comparison, these characteristics of $La_{0.825}Sr_{0.175}MnO_3$ (LSMO) are presented as well.

2. Experiment

A series of samples $La_{0.7}Ca_{0.3-x}Sr_xMnO_3$ ($x = 0.1$, 0.12, 0.135, and 0.15) and $La_{0.825}Sr_{0.175}MnO_3$ are synthesized by a conventional solid–state reaction method at high temperature. The La_2O_3, $CaCO_3$, $SrCO_3$, and MnO_2 (99.99% purity) powders are used as raw materials during the solid-state reaction processing. The powder of La_2O_3 is pre-heated at 1273 K for 8 h before weighed. The other raw materials are also dried at 423 K for 4 h to remove the moisture content. These raw materials are ground for 8 h with the ethanol. After dried, the powder mixtures are fired repeatedly in the muffle furnace for 20 h at 1273 K. The resultant powders are pressed into pellets 40 mm in diameter and 4 mm thick. The pellets are then sintered for 22 h in air at temperatures 1723 K. After cooled to room temperature, the as-prepared pellets are annealed in a flowing oxygen atmosphere of 20 ml/min at 1273 K for 10 h. Finally, the test samples are machined and polished into discs with 25 mm in diameter and 0.4 mm thick.

The structure of samples is characterized by X-ray diffraction (XRD, D8 ADVANCE, Bruker Co., Germany) with Cu-Kα radiation at room temperature. Microstructure of samples is analyzed by field-emission scanning electron microscopy (SEM, S-4800, Hitachi Co., Japan) before polished. The root-mean-square (RMS) roughness of the polished samples is detected by atomic force microscopy (AFM, CSPM4000, Being Ltd., China). The electrical resistivity of the samples, as a function of temperature, is measured with a physical property measurement system (PPMS-14, Quantum Design Co., America) from 150 K to 350 K using the standard four probe ac method. The accessory of Transmission-Reflection Dewar (Catalog No. DER-300, Harrick Scientific Products, Inc., America) is mounted directly in the FT-IR spectrometer (VERTEX80v, Bruker Co., Germany) to measure the temperature-dependent infrared spectra (15° incident angles, 16 scans, resolution 2 cm^{-1}) of all samples over the range from 4000 to 400 cm^{-1}. Temperature of these samples from 97 K to 373 K is controlled using liquid nitrogen and two heating cartridges. A gold film is employed as a reference mirrors to determine the reflectivity.

3. Measuring methods of emissivity

Generally, there are three methods to measure the emissivity, i.e. direct measurement, indirect measurement from the reflectivity spectra and calorimetric measurement [10–12]. For opaque manganese oxides, indirect measurement is a good alternative to determine the emissivity because a reflectivity measurement is currently performed. From a radiation balance on a certain medium, the flux of radiation can be expressed as follows

$$\rho_\lambda + \alpha_\lambda + \tau_\lambda = 1, \tag{1}$$

where ρ_λ, α_λ, and τ_λ is the spectral reflectivity, the spectral absorptivity, and the spectral transmissivity of the flow respectively. For an opaque materials, there is no transmission, and the absorption and reflection are surface processes for which $\rho_\lambda + \alpha_\lambda = 1$. According to Kirchoff's law, the spectral emissivity ε_λ can be deduced from spectral reflectivity. It follows that $\alpha_\lambda = 1-\rho_\lambda = \varepsilon_\lambda$.

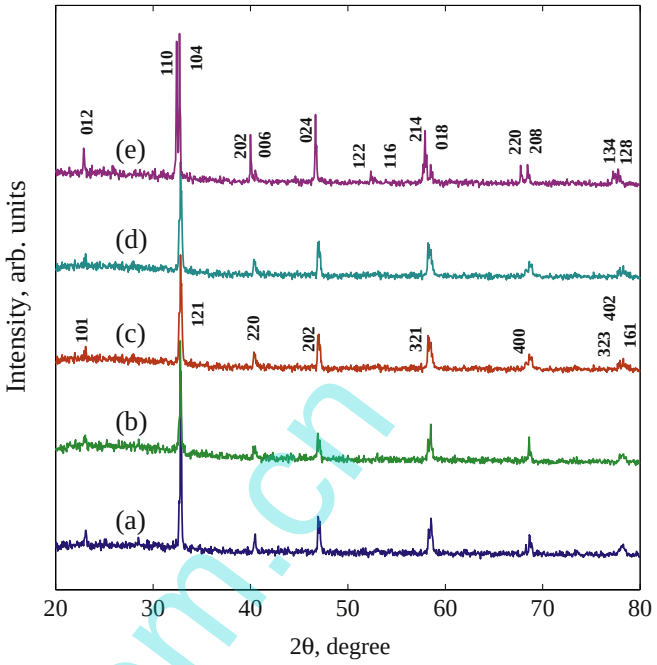

Fig. 1. XRD patterns of (a) $La_{0.7}Ca_{0.2}Sr_{0.1}MnO_3$, (b) $La_{0.7}Ca_{0.18}Sr_{0.2}MnO_3$, (c) $La_{0.7}Ca_{0.165}Sr_{0.135}MnO_3$, (d) $La_{0.7}Ca_{0.15}Sr_{0.15}MnO_3$, and (e) $La_{0.825}Sr_{0.175}MnO_3$.

For a sample with the temperature-dependent infrared reflectivity spectra, its infrared emissivity can be obtained by integrating the spectral reflectivity in the wavelength range from 2.5 μm (4000 cm^{-1}) to 25 μm (400 cm^{-1}) as follows:

$$\varepsilon(T) = \frac{\int_{2.5}^{25} [1-\rho(\lambda,T)]E_{\lambda,b}(\lambda,T)\mathrm{d}\lambda}{\int_{2.5}^{25} E_{\lambda,b}(\lambda,T)\mathrm{d}\lambda}. \tag{2}$$

Where $E_{\lambda,b}(\lambda,T) = C_1\lambda^{-5}[\exp(C_2/\lambda T)-1]^{-1}$, the value of first and second radiation constants is $C_1 = 3.742 \times 10^8$ W μm^4/m^2 and $C_2 = 1.439 \times 10^4$ mK, respectively.

In this work, the temperature-dependent reflectivity spectra $\rho(\lambda,T)$ are measured by experiment. In the temperature range of 97–373 K, we take 89% of the radiant energy of blackbody at 373 K with wavelengths between 2.5 μm and 25 μm into account.

4. Results and discussions

The structure of all samples is characterized by powder XRD at room temperature. The XRD patterns (in Fig. 1) show that all the samples are single phase, and exhibit the characteristic peaks of the perovskite structure. Table 1 lists the structure parameters and the

Table 1
Structure parameters and metal–insulator transition temperature for the samples.

Sample	Space group	Lattice parameters (Å)			T_{MI} (K)
		a	*b*	*c*	
$La_{0.7}Ca_{0.2}Sr_{0.1}MnO_3$	*Pnma*	5.4489	7.7209	5.4932	251
$La_{0.7}Ca_{0.18}Sr_{0.12}MnO_3$	*Pnma*	5.4477	7.6931	5.501	270
$La_{0.7}Ca_{0.165}Sr_{0.135}MnO_3$	*Pnma*	5.4566	7.7171	5.5024	295
$La_{0.7}Ca_{0.15}Sr_{0.15}MnO_3$	$R\bar{3}c$	5.4719	–	13.3198	301
$La_{0.825}Sr_{0.175}MnO_3$	$R\bar{3}c$	5.527	–	13.3452	281

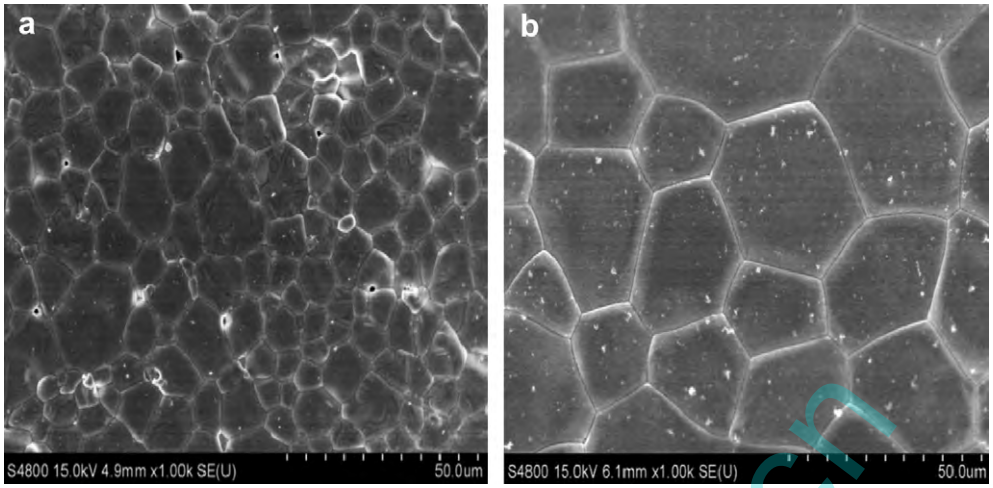

Fig. 2. SEM photographs of the LSMO with sintering temperature (a) 1623 K and (b) 1723 K.

metal–insulator transition temperature T_{MI}, which are determined by the XRD data and the temperature-dependent resistivity for all samples, respectively. The LCSMO samples with $x = 0.1$, 0.12, and 0.135 are orthorhombic phase with *pnma* space group, while the $x = 0.15$ and LSMO samples are rhombohedral phase with $R\bar{3}c$ space group. With increasing doping level x, the crystal structure of LCSMO samples varies from orthorhombic phase ($x < 0.15$) to rhombohedral phase ($x = 0.15$) at room temperature. The result is fully identical with those reports in previous works [13,14].

SEM photographs of LSMO sample at different sintering temperature (1623 K and 1723 K) are shown in Fig. 2. Grains about 7 μm with some pores can be observed at sintering temperature 1623 K. However, pores are not found and large grains about 15 μm are formed at sintering temperature 1723 K. This means that 1723 K sintering is high enough for grain growth and densification in doped lanthanum manganites.

The surface of sample is polished before measured the infrared spectra. The RMS roughness of the polished sample $La_{0.7}Ca_{0.2}Sr_{0.1}MnO_3$, which is accessed from AFM, is 0.557 nm. Its AFM image, in Fig. 3, shows that the surface of sample is dense and uniform. No cracks or defects have been observed.

Fig. 4 shows the temperature dependence of zero field resistivity for all samples measured at 150–350 K. It is observed that all the samples show an intrinsic metal–insulator transition at a temperature T_{MI}, which results from the double exchange effects of the doped lanthanum manganites. The transition temperature T_{MI} as shown Table 1 increases from 251 K to 301 K with increasing doping concentration x in LCSMO. This is similar to the reports of $La_{0.8}Ca_{0.2-x}Sr_xMnO_3$ [15]and LCSMO samples [16]. The T_{MI} of LCSMO ($x = 0.135$) sample is close to room temperature. It is interesting to notice that a second peak is found for the LCSMO ($x = 0.135$ and 0.15) samples at temperature bellow T_{MI}. This behavior may be attributed to a small grain size in polycrystalline samples [17–19] and can be explained by the model proposed by Zhang et al. [17]. In this model, the peak at high temperature reflects the intrinsic characteristics of metal–insulator transition, whereas the second peak is considered as an interfacial tunneling feature.

The variation in infrared spectral reflectivity with temperature for the selected samples is shown in Fig. 5. The reflectivity spectra of all samples show an overall decreasing trend upon heating. From the figure, it can be seen that the reflectivity spectra display a large variation with temperature below T_{MI} and are almost no change above T_{MI}. In addition, above and near T_{MI}, the spectra show a nonmetal behavior with sharp reflection peaks at the wavenumber of 590 cm^{-1}. For higher wavenumber, these samples should present two absorption bands at around 357 cm^{-1} and 167 cm^{-1}, related to the internal motion of Mn–O–Mn bond and deformation modes of the MnO_6 octahedra, respectively [20–22]. The observed reflection peaks at 590 cm^{-1} are caused by the

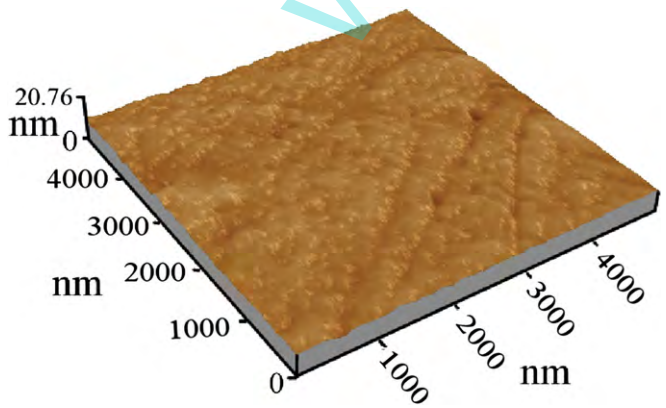

Fig. 3. Three dimension AFM of $La_{0.7}Ca_{0.2}Sr_{0.1}MnO_3$.

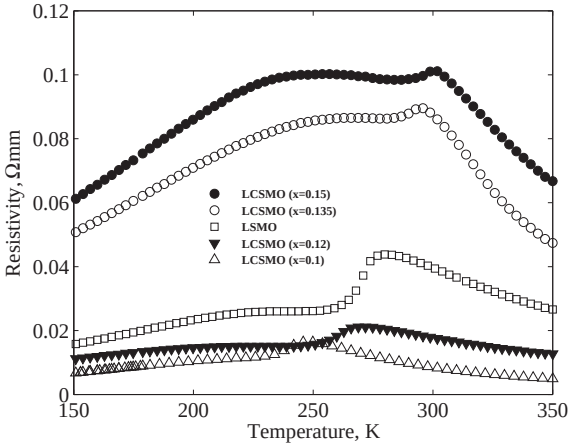

Fig. 4. Resistivity versus temperature for $La_{1-x}A_xMnO_3$ samples in zero magnetic fields.

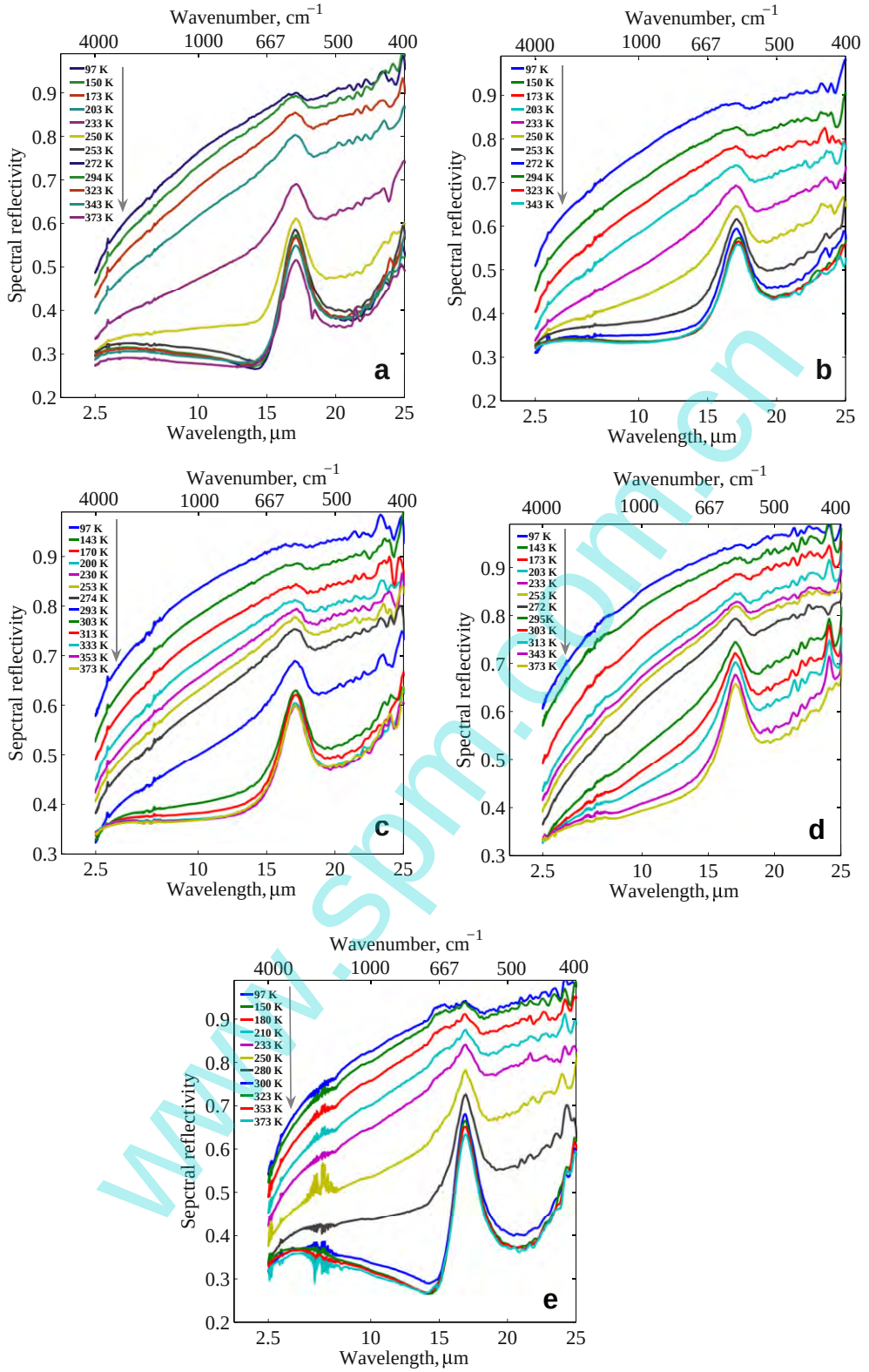

Fig. 5. Temperature-dependent infrared reflectivity spectra of (a) $La_{0.7}Ca_{0.2}Sr_{0.1}MnO_3$ (b) $La_{0.7}Ca_{0.18}Sr_{0.2}MnO_3$, (c) $La_{0.7}Ca_{0.165}Sr_{0.135}MnO_3$, (d) $La_{0.7}Ca_{0.15}Sr_{0.15}MnO_3$, and (e) $La_{0.825}Sr_{0.175}MnO_3$.

absorptions of optical phonons corresponding to Mn–O stretching vibrations. As the temperature decreases, the reflectivity gradually increases and the phonon peaks become smooth gradually due to the dielectric screening effect. This is consistent with the report of $La_{0.825}Sr_{0.175}MnO_3$ [23]. The reflectivity of all the samples at low temperature (97 K) is higher than at high temperature (373 K). This reveals that the spectral reflectivity shows a transition of metal–insulator with temperature. Some disturbances around the

wavelength of 5 μm in the Fig. 5(e) may be attributed to the window fogging of KBr during test.

The infrared emissivity in the temperature region of 97–373 K is deduced from the experimental reflectivity spectra using Eq. (2) as shown in Fig. 6. It is observed that the emissivity of these manganese oxides material increases with increasing temperature and undergoes a sharp variation in the vicinity of T_{MI} due to the metal–insulator transition [24]. The results are similar to those reported by K. Shimazaki et al. [25]and G. Tang et al. [3,5,26]. In $La_{1-x}Sr_xMnO_3$ materials, G. Tang et al. [3] have reported that the emissivity of materials below the T_{MI} decreases with the increase of the Sr^{2+} doping concentration due to the enhanced metallic properties. In our samples, however, it can be seen from the Fig. 6 that the emissivity of LCSMO ($x = 0.1$) sample is lower than the LCSMO ($x = 0.12$) sample below T_{MI}. The reason may be attributed to the surface condition of LCSMO ($x = 0.1$) sample. K. Shimazaki et al. [25] have discussed the role of the surface condition in LSMO manganese oxides. They obtained three kinds of surface conditions for LSMO samples possessing different RMS roughness value. The RMS roughness values of the three samples were 107 nm, 17 nm, and 1.4 nm, respectively. Interestingly, comparing with the other samples, the emissivity of the sample with an RMS roughness of 1.4 nm is the lowest at low temperature, whereas three samples have almost no change at high temperature. Therefore, for the LCSMO ($x = 0.1$) sample in this work, such small RMS roughness of 0.557 nm as shown in Fig. 3 tends to have a lower emissivity than that of the LCSMO ($x = 0.12$) sample at low temperature zone.

The inset of Fig. 6 represents the relationship between infrared emissivity with different temperature and doping level (x) in LCSMO samples. It can be seen from the figure that the infrared emissivity of sample decreases with increasing doping level (x). For example, the emissivity decreases from 0.65 ($x = 0.1$) to 0.31 ($x = 0.15$) at the temperature of 273 K. The reason is that the increase of doping level (x) leads to rising mobility of free electron, thus results in the decrease of infrared emissivity [7]. The emissivity decreases slightly with increasing doping level (x) at the temperature of 97 K and 373 K. This may be because these samples are in a thorough metallic state at 97 K and in a near thorough insulator state at 373 K.

Table 2 lists the infrared emissivity of all samples at 97 K (ε), 173 K (ε), and 373 K (ε), respectively; and the variation amplitude of their respective emissivity in the 97–373 K range ($\Delta\varepsilon$) and in 173–373 K range($\Delta\varepsilon$). It is found that the emissivity of all samples at 97 K shows metallic property with a low emissivity value about 0.1 and at 373 K is in insulator state with a high emissivity value over 0.6. For the LCSMO ($x = 0.135$) sample, its emissivity increases from 0.04 at 97 K to 0.57 at 373 K and the variation amplitude of its emissivity is 0.53 in this temperature range, especially its transition temperature T_{MI} = 295 K is close room temperature. For the LCSMO ($x = 0.1$) and LSMO samples, the variation amplitude of emissivity in the range of 97–373 K is close to the value of 0.6, which is by far the largest reported value among the doped manganese oxides material. Comparing with the previous works [3,25,27], it can be found from Table 2 that the variation amplitude of emissivity is enhanced for the LSMO sample in the temperature range of 173–373 K. There may be two reasons for the enhancement. On the one hand, densification, which is achieved at sintered temperature as high as 1723 K, reduces the gaps between grains and increases mobility of free electrons below transition temperature. The increased mobility of free electrons results in a lower emissivity. On the other hand, a smaller RMS roughness of polished sample can also obtain a lower emissivity below transition temperature.

Table 2
The infrared emissivity of samples at various temperatures and its variation amplitude.

Sample	ε_{97}	ε_{173}	ε_{373}	$\Delta\varepsilon_1$	$\Delta\varepsilon_2$	Reference
$La_{0.7}Ca_{0.2}Sr_{0.1}MnO_3$	0.09	0.19	0.69	0.6	0.5	This work
$La_{0.7}Ca_{0.18}Sr_{0.12}MnO_3$	0.1	0.25	0.61	0.51	0.36	This work
$La_{0.7}Ca_{0.165}Sr_{0.135}MnO_3$	0.06	0.18	0.6	0.54	0.42	This work
$La_{0.7}Ca_{0.15}Sr_{0.15}MnO_3$	0.04	0.14	0.57	0.53	0.43	This work
	0.06	0.13	0.65	0.59	0.52	This work
$La_{0.825}Sr_{0.175}MnO_3$	–	0.21	0.63	–	0.42	[4,25]
	–	0.38	0.75	–	0.37	[3]

The above results show that the emissivity of LCSMO material can be self-adjusted basing on temperature change. This emissivity tunable properties is useful to improve the temperature fluctuation of spacecraft for varying operating conditions. Fig. 7 shows a schematic of the operation of LCSMO material above T_{MI} (high emissivity state) and below T_{MI} (low emissivity state). When the spacecraft temperature increases over T_{MI}, emissivity of the material increases. Thereby, the amount of heat radiation to space environment increases and lowers the surface temperature.

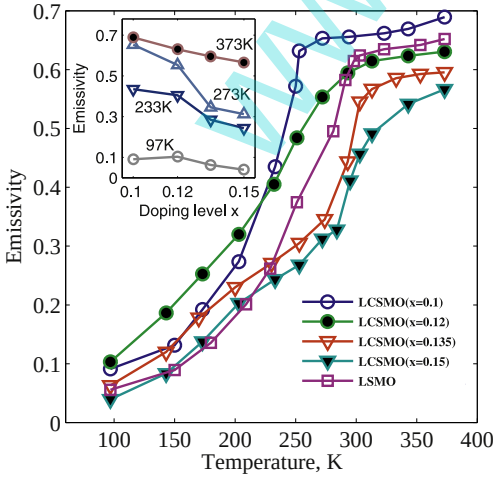

Fig. 6. Temperature dependence of infrared emissivity calculated by Eq. (2) for all samples. The inset shows the relationship between infrared emissivity at different temperature and doping level (x) for samples $La_{0.7}Ca_{0.3-x}Sr_xMnO_3$.

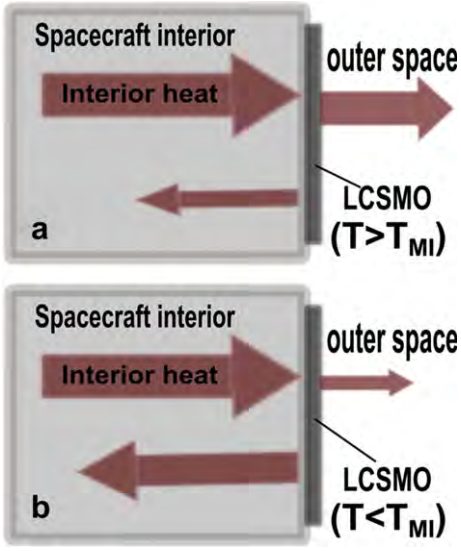

Fig. 7. Schematic of operation of thermal control material $La_{0.7}Ca_{0.3-x}Sr_xMnO_3$.

Conversely, by keeping a low emissivity to space environment below T_{MI}, the material enhances the self-heating of the spacecraft to reduce interior heating requirements. Moreover, the material has a well durability to proton, electron and UV radiation, which is reported by S. Tachikawa et al. [28,29]. What's more, the usage of LCSMO material can reduce or eliminate the need for auxiliary heaters during spacecraft in cold environments.

Spacecraft thermal control materials are described by their emissivity and by their heat rejection capacity, which is the power they are capable of radiating. The heat rejection capacity $\dot{Q}$ (W) can be represented by Eq. (3). Here, σ is the Stefan–Boltzmann constant (5.67×10^{-8} W/m^2 K^4), A(m^2) is the thermal control surface area, T_s is the thermal control surface temperature, T_b is the space background temperature (4 K), ε is the emissivity of the thermal control material, α is the solar absorptivity of the thermal control material, q_{IR} is the infrared earth radiation, and the S is the solar constant.

$$\frac{\dot{Q}}{A} = \varepsilon\sigma\left(T_s^4 - T_b^4\right) - \alpha q_{IR} - \alpha S. \tag{3}$$

This is only a simplified model to account for a thermal control application. If spacecraft operates in 550 km orbit, the infrared earth radiation q_{IR} would be about 200 W/m^2 [1] and the term of solar radiation αS can be neglected when it is on the shady side of earth. For the LCSMO material, its solar absorptivity is very large, but the solar absorptivity can be reduce to 0.28 by depositing solar reflection films on its surface in our pervious work [30]. Here, we calculated the heat rejection density $\dot{Q}/A$ of three thermal control materials (Aluminum, OSR, and $La_{0.7}Ca_{0.165}Sr_{0.135}MnO_3$, respectively) to evaluate their application performance. The calculated results are show in Fig. 8. If the temperature of spacecraft surface is limited in the range of 250–300 K, which in the vicinity of T_{MI} of LCSMO material, one expects a large enough heat rejection density above 300 K and a small enough heat rejection density or a suitable heating below 250 K. From the Fig. 8, it can be found that OSR ($\varepsilon = 0.8$, $\alpha = 0.1$) and Aluminum ($\varepsilon = 0.04$, $\alpha = 0.15$) are the expected thermal control materials above 300 K and below 250 K, respectively. Unfortunately, the usage of OSR requires an auxiliary heater when the temperature is low to 250 K and the usage of Aluminum is need to an auxiliary cooler above 300 K. This means an additional power consumption and moving parts are required. It is observed that the heat rejection density of LCSMO is negative below 250 K ($\dot{Q}/A < 0$) This means that the usage of LCSMO can self-heating the spacecraft surface below 250 K to reduce or avoid heater requirement. In spite of the heat rejection density of LCSMO is lower than that of OSR above 300 K, the LCSMO can be used without heater below 250 K. Comparing to Aluminum and OSR, therefore, the LCSMO thermal control material is more advantageous. This results suggest that the LCSMO can be used in the spacecraft thermal control.

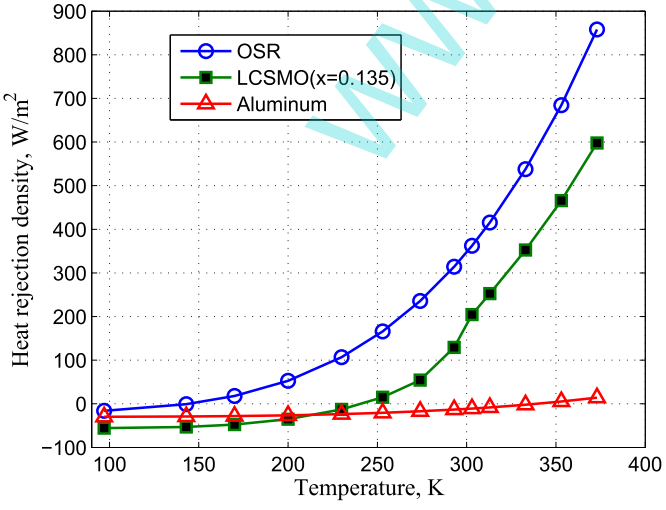

Fig. 8. Heat rejection density calculated by Eq. (3) for selected thermal control materials.

5. Conclusions

In this work, we synthesized $La_{0.7}Ca_{0.3-x}Sr_xMnO_3$ compositions which exhibit a tunable infrared properties basing on its temperature. The transition temperature T_{MI} can be adjusted close to room temperature for$La_{0.7}Ca_{0.165}Sr_{0.135}MnO_3$. The temperature-dependent infrared reflectivity spectra, which decrease with increasing temperature, show a metallic character below T_{MI} and an insulator character above. The infrared emissivity of all the samples can be self-adjusted with the variation of temperature, just like the emissivity of $La_{0.7}Ca_{0.2}Ca_{0.1}MnO_3$ varies from 0.09 at 97 K to 0.69 at 373 K. The tunable properties of infrared emissivity with temperature make the compositions attractive for applications as thermal control material in space.

Acknowledgements

This work is sponsored by the National Science Foundation of China (Grant nos. 50936002 and 51225602).

References

[1] V. Baturkin, Micro-satellites thermal control–concepts and components, Acta Astronaut. 56 (2005) 161–170.
[2] P. Laffez, M. Zaghrioui, L. Reversat, P. Ruello, Electron doped $Sm_{1-x}Ca_xMnO_3$ perovskite manganite as potential infrared thermochromic switch, Appl. Phys. Lett. 89 (2006) 081909.
[3] G. Tang, Y. Yu, Y. Cao, W. Chen, The thermochromic properties of $La_{1-x}Sr_xMnO_3$ compounds, Sol. Energy. Mater. Sol. Cells 92 (2008) 1298–1301.
[4] K. Shimazaki, S. Tachikawa, A. Ohnishi, Y. Nagasaka, Radiative and optical properties of $La_{1-x}Sr_xMnO_3$ ($0<x<0.4$) in the vicinity of metalcinsulator transition temperatures from 173 to 413 K, Int. J. Thermophys 22 (2001) 1549–1561.
[5] G. Tang, Y. Yu, W. Chen, Y. Cao, The electrical resistivity and thermal infrared properties of $La_{1-x}Sr_xMnO_3$ compounds, J. Alloys. Compd 461 (2008) 486–489.
[6] C. Wu, J. Qiu, J. Wang, M. Xu, L. Wang, Thermochromic property of $La_{0.8}Sr_{0.2}MnO_3$ thin-film material sputtered on quartz glass, J. Alloys. Compd 506 (2010) L22–L24.
[7] X. Shen, G. Xu, C. Shao, Influence of structure on infrared emissivity of lanthanum manganites, Physica B 405 (2010) 1090–1094.
[8] J. Huang, Y. Xuan, Q. Li, Perovskite-type oxide films combined with gratings for reduction of material consumption and improvement of thermochromism property, J. Quant. Spectrosc. Radiat. Transfer 112 (2011) 2592–2599.
[9] F. Yonglai, C.K. Ong, The magnetoresistance effect of La–Ca–Sr–Mn–O perovskites under a very low magnetic field, J. Magn. Magn. Mater. 208 (2000) 69–73.
[10] P. Herve, N. Rambure, A. Sadou, D. Ramel, L. Francou, P. Delouard, E. Gavila, Direct measurement of total emissivities at cryogenic temperatures: application to satellite coatings, Cryogenics 48 (2008) 463–468.
[11] C. Napierala, M. Edely, P. Laffez, L. Sauques, Thermo-optical effect of $Nd_{0.3}Sm_{0.7}NiO_3$ ceramic in the infrared range, Opt. Mater. 31 (2009) 1498–1501.
[12] C. Fabron, A. Meurat, Measurements of Total Hemispheric Emissivity at Low Temperatures-designing a Cryogenic Test Bench, in: 4th International Symposium Environmental Testing for Space Programmes, ESA, Liège, Belgium, 2001, pp. 51–59.
[13] Y. Tomioka, A. Asamitsu, Y. Tokura, Magnetotransport properties and magnetostructural phenomenon in single crystals of $La_{0.7}(Ca_{1-y}Sr_y)_{0.3}MnO_3$, Phys. Rev. B 63 (2000). 024421–1–6.
[14] A.N. Ulyanov, J.S. Kim, Y.M. Kang, D.G. Yoo, S.I. Yoo, Oxygen deficiency as a driving force for metamagnetism and large low field magnetocaloric effect in $La_{0.7}Ca_{0.3-x}Sr_xMnO_3$ manganites, J. Appl. Phys. 104 (113916) (2008) 1–7.
[15] G. Garbarino, C. Acha, A phenomenological model for the pressure sensitivity of the curie temperature in hole-doped manganites, Europhys. Lett. 88 (2009). 46003–1–6.
[16] Y.-M. Kang, N.-H. Ka, D.-G. Yoo, G.-M. Shin, K.-P. Ko, S.-I. Yoo, Magnetotransport properties of $La_{0.7}Ca_{0.3-x}Sr_xMnO_3$ thin films deposited by pulsed electron deposition, IEEE Trans. Magn. 45 (2009) 2572–2575.

[17] N. Zhang, W. Ding, W. Zhong, D. Xing, Y. Du, Tunnel-type giant magnetoresistance in the granular perovskite $La_{0.85}Sr_{0.15}MnO_3$, Phys. Rev. B 56 (1997) 8138–8142.
[18] P. Kameli, H. Salamati, A. Aezami, Influence of grain size on magnetic and transport properties of polycrystalline $La_{0.8}Sr_{0.2}MnO_3$ manganites, J. Alloys. Compd 450 (2008) 7–11.
[19] N. Ibrahim, A.K. Yahya, S.S. Rajput, S. Keshri, M.K. Talari, Double metal-insulator peaks and effect of Sm^{3+} substitution on magnetic and transport properties of hole-doped $La_{0.85}Ag_{0.15}MnO_3$, J. Magn. Magn. Mater. 323 (2011) 2179–2185.
[20] T.-h. Arima, Y. Tokura, optical study of electronic structure in perovskite-type RMO_3 (R=La, Y; M=Sc, Ti, V, Cr, Mn, Fe, Co, Ni, Cu), J. Phys. Soc. Jpn. 64 (1995) 2488–2501.
[21] K.H. Kim, J.Y. Gu, H.S. Choi, G.W. Park, T.W. Noh, Frequency shifts of the internal phonon modes in $La_{0.7}Ca_{0.3}MnO_3$, Phys. Rev. Lett. 77 (1996) 1877–1880.
[22] G.D. Marzi, Z.V. Popović, A. Cantarero, Z. Dohčević-Mitrović, N. Paunović, J. Bok, F. Sapiña, Effect of a-site and b-site substitution on the infrared reflectivity spectra of $La_{1-y}A_yMn_{1-x}B_xO_3$ (A=Ba, Sr; B=Cu, Zn, Sc; $0<y<0.3$; $0<x<0.1$) manganites, Phys. Rev. B 68 (2003). 064302–64311–7.
[23] Y. Okimoto, T. Katsufuji, T. Ishikawa, A. Urushibara, T. Arima, Y. Tokura, Anomalous variation of optical spectra with spin polarization in double-exchange ferromagnet $La_{1-x}Sr_xMnO_3$, Phys. Rev. Lett. 75 (1995) 109–112.
[24] K. Shimazaki, A. Ohnishi, Y. Nagasaka, Development of spectral selective multilayer film for a variable emittance device and its radiation properties measurements, Int. J. Thermophys 24 (2003) 757–769.
[25] K. Shimazaki, S. Tachikawa, A. Ohnishi, Y. Nagasaka, Temperature dependence of total hemispherical emittance in perovskite-type manganese oxides, $La_{1-x}Sr_xMnO_3$, High Temp. High Pressures 33 (2001) 525–531.
[26] G. Tang, Y. Yu, W. Chen, Y. Cao, Thermochromic properties of manganese oxides $La_{1-x}A_xMnO_3$ (A=Ca, Ba), Mater. Lett. 62 (2008) 2914–2916.
[27] X. Shen, G. Xu, C. Shao, C. Cheng, Temperature dependence of infrared emissivity of doped manganese oxides in different wavebands (3–5 and 8–14)μm, J. Alloys. Compd 479 (2009) 420–422.
[28] S. Tachikawa, A. Ohnishi, K. Shimazaki, A. Okamoto, Y. Nakamura, Y. Shimakawa, T. Manako, T. Mori, A. Ochi, Development of a variable emittance radiator, in: 29th International Conference on Environment Systems, SAE, Denver, Colorado, 1999.
[29] S. Tachikawa, A. Ohnishi, Y. Shimakawa, A. Ochi, A. Okamoto, Y. Nakamura, Development of a variable emittance radiator based on a perovskite manganese oxide, in: 8th AIAA/ASME Joint Thermophysics and Heat Transfer Conference, AIAA, Louis, Missouri, 2002, pp. 24–26.
[30] D. Fan, Q. Li, Y. Xuan, Tailoring the solar absorptivity of thermochromic material $La_{0.7}Ca_{0.2}Sr_{0.1}MnO_3$, J. Quant. Spectrosc. Radiat. Transfer 112 (2011) 2794–2800.